Probing unconventional superconductivity in inversion-symmetric doped Weyl semimetal

Youngseok Kim,[1] Moon Jip Park,[2] and Matthew J. Gilbert[1,3]
[1]*Department of Electrical and Computer Engineering, University of Illinois, Urbana, Illinois 61801, USA*
[2]*Department of Physics, University of Illinois, Urbana, Illinois 61801, USA*
[3]*Micro and Nanotechnology Laboratory, University of Illinois, Urbana, Illinois 61801, USA*
(Received 11 April 2016; revised manuscript received 1 June 2016; published 20 June 2016)

Unconventional superconductivity has been predicted to arise in the topologically nontrivial Fermi surface of doped inversion-symmetric Weyl semimetals (WSMs). In particular, Fulde-Ferrell-Larkin-Ovchinnikov (FFLO) and nodal BCS states are theoretically predicted to be possible superconductor pairing states in inversion-symmetric doped WSMs. In an effort to resolve the preferred pairing state, we theoretically study two separate four-terminal quantum transport methods that each exhibit a unique electrical signature in the presence of FFLO and nodal BCS states in doped WSMs. We first introduce a Josephson junction that consists of a doped WSM and an *s*-wave superconductor in which we show that the application of a transverse uniform current in *s*-wave superconductors effectively cancels the momentum carried by FFLO states in doped WSMs. From our numerical analysis, we find a peak in Josephson current amplitude at finite uniform current in *s*-wave superconductors that serves as an indicator of FFLO states in doped WSMs. Furthermore, we show using a four-terminal measurement configuration that the nodal points may be shifted by an application of transverse uniform current in doped WSMs. We analyze the topological phase transitions induced by nodal pair annihilation in nonequilibrium by constructing the phase diagram and we find a characteristic decrease in the density of states that serves as a signature of the quantum critical point in the topological phase transition, thereby identifying nodal BCS states in doped WSMs.

DOI: 10.1103/PhysRevB.93.214511

I. INTRODUCTION

Rapid progress in the field of topological phases of matter has extended the scope of our understanding from fully gapped insulators to gapless semimetals [1–3], an example of which is the Weyl semimetal (WSM), whose low-energy excitations are described by three-dimensional Weyl fermions [1,2]. The WSM is characterized by its nondegenerate band crossing points referred to as Weyl nodes, where the valence and conduction band touch. Weyl nodes are monopoles of the Berry curvature in momentum space [1,4] and the Fermi surface (FS) enclosing the Weyl node is topologically nontrivial as it carries monopole charge (or Chern number). Weyl nodes with opposite monopole charge appear in pairs in the lattice [5,6] and the pairs of Weyl nodes are responsible for emergent phenomena such as Fermi arcs [2,7,8] and unconventional electromagnetic responses such as negative magnetoresistance and chiral magnetic effect [9].

The unique physics of WSM motivates further research on one of the most striking differences between semimetals and insulators: the *intrinsic* superconducting phases in doped semimetals. Unconventional superconductivity has been shown to arise from the interplay between topologically nontrivial states and superconducting phases of doped WSMs [10–15]. Specifically, as FSs enclosing Weyl nodes must appear in even numbers [5,6], doped WSMs facilitate two types of possible superconducting pairings: internode and intranode pairing. When Weyl nodes with opposite monopole charge are mapped to each other by inversion symmetry, the internode pairing exhibits a nodal BCS pairing state whose electrical structure is in close analogy with the ^{3}He-*A* phase [10,16,17]. On the other hand, the intranode pairing forms finite momentum carrying superconducting states [10] known as the Fulde-Ferrell-Larkin-Ovchinnikov (FFLO) states [18,19]. While both types of superconducting states are possible, different analysis methods yield different energetically preferred pairing states [10–13]. Assuming even-parity pairing (singlet) states in low-energy chiral basis, mean-field calculations show that FFLO pairing is favored [10]. On the contrary, when one considers odd-parity pairing (triplet), a short- and long-range attractive interaction results in FFLO and BCS pairing states as ground states, respectively [11]. In the weak-coupling regime, BCS states are energetically preferred; however, FFLO states may have lower energy in the absence of both inversion and time-reversal symmetry, due to the fact that FFLO states rely on low-energy chiral symmetry while electrons in the BCS states are connected either by inversion or time-reversal symmetry [12].

Although finding energetically preferred pairing is crucial to clarify microscopic details of the superconductivity, it is unclear how to determine a pairing scheme for a given doped WSM. In this regard, we propose a quantum transport method to elucidate the pairing states in doped WSMs. More precisely, we focus our discussion on inversion-symmetric doped WSMs and on two possible unconventional superconducting states: FFLO and nodal BCS states. To identify two seemingly distinct superconducting states, we propose two complementary transport methods. In Sec. II, we introduce a Josephson junction composed of a doped WSM and a conventional *s*-wave superconductor in the weak-coupling regime to resolve the FFLO states. We find that the Josephson current is averaged out to be vanishingly small due to the spatially oscillating order parameter of FFLO states. By driving transverse supercurrent in *s*-wave superconductors, we show that nonequilibrium *s*-wave pairing states mimic FFLO states and the Josephson current is restored at finite transverse current, which serves as a signature for FFLO pairing in doped WSMs. In Sec. III, we introduce a system consisting of a doped WSM attached with

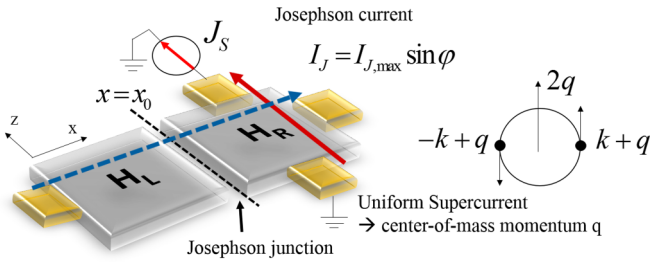

FIG. 1. A schematic of the system. H_L is a WSM and H_R is an ordinary metal superconductor. A weak coupling between H_L and H_R is assumed. A Josephson current flows in the $\hat{x}$ direction (blue dashed arrow) and a uniform supercurrent in the $\hat{z}$ direction (red solid arrow) gives center-of-mass momentum q to the H_R system.

four-terminal contacts to identify nodal BCS states. We show that nodal points are shifted in momentum space by tuning transverse dc current, which may result in an annihilation of nodal points and a subsequent topological phase transition. At the critical point of the topological phase transition, we find a distinct peak in the longitudinal differential conductance (dI/dV) curve inside the superconducting gap that serves as a signature of the nodal BCS states in doped WSMs. In Sec. IV, we summarize our results and conclude.

II. PROBING FFLO PAIRING STATES

A. System description

In Fig. 1, we consider a Josephson junction that consists of a doped WSM (H_L) weakly coupled with a conventional s-wave superconductor (H_R). When the system is in the superconducting regime, a Josephson current flows in the longitudinal ($\hat{x}$) direction, as shown by the blue dashed arrow in Fig. 1, across the junction located at $x = x_0$. The doped inversion-symmetric WSM system in this work has two Weyl nodes located at $\pm\mathbf{Q}$ in momentum space. Assuming internode pairing, a Cooper pair that shares a FS with momenta $\pm\mathbf{Q}+\mathbf{k}$ and $\pm\mathbf{Q}-\mathbf{k}$ forms an FFLO state [10]. Therefore, a net momentum of $\pm 2\mathbf{Q}$ is carried by the pairing states and the order parameter of the FFLO states has a form $\Psi_L(\mathbf{r}) = \psi_L(e^{i2\mathbf{Q}\cdot\mathbf{r}} + e^{-i2\mathbf{Q}\cdot\mathbf{r}})$ in real space, where ψ_L is an amplitude of the order parameter [18,19]. Assuming uniform BCS pairing for the s-wave superconductor, the superconducting order parameter is $\Psi_R(\mathbf{r}) = \psi_R$ and the total Josephson current may be determined as [20]

$$I_J \propto \mathrm{Im}\left[\psi_L\psi_R\int d^2\mathbf{r}e^{i(2\mathbf{Q}\cdot\mathbf{r}+\delta\varphi)} + e^{i(-2\mathbf{Q}\cdot\mathbf{r}+\delta\varphi)}\right], \quad (1)$$

where $\delta\varphi$ is relative phase difference of two superconducting systems, and the integral covers the entire interface of the Josephson junction. In Eq. (1), I_J vanishes as one integrates over $\mathbf{r}$ due to the spatially oscillating FFLO state order parameter. However, previous work [20] shows that one may effectively cancel the finite momentum $\mathbf{Q}$ by introducing external magnetic field and, as a result, the Josephson current is restored. Although the nonzero Josephson current under applied magnetic field can be utilized to identify FFLO states, the same proposal may not be applicable in the WSM. In the presence of a magnetic field, the low-energy Hamiltonian of the WSM leaves only a 1D chiral mode in the lowest Landau level [21] and, therefore, the intranode coupling cannot occur. To overcome this situation, we show that a driven supercurrent plays the role of the magnetic field.

The red solid arrow in Fig. 1 shows a uniform supercurrent flowing within the s-wave superconductor. We consider a planar geometry where a bias is applied to metal contacts and drives a uniform current through the sample. Regardless of the bias applied to the other contacts for measurement, a constant transport current may be induced in the sample by using external bias [22,23]. In the presence of a uniform supercurrent, a Cooper pair acquires a finite center-of-mass momentum $\mathbf{q}$. Then electrons at $\mathbf{k}+\mathbf{q}$ and $-\mathbf{k}+\mathbf{q}$ constitute a Cooper pair with a net momentum of $2\mathbf{q}$. As a result, the s-wave pairing states under nonequilibrium effectively mimic finite-momentum carrying FFLO states with the order parameter [24,25] $\Psi_R = \psi_R e^{i2\mathbf{q}\cdot\mathbf{r}}$. Especially when the momentum $\mathbf{q}$ is parallel to and in a resonance with $\mathbf{Q}$ carried by the FFLO states, the Josephson junction has a nonvanishing I_J, which may serve as a signature of FFLO states in doped WSMs. In the above scenario, a uniform transverse current, $\mathbf{J}_S$, is carried by Cooper pairs with finite net momentum $2\mathbf{q}$, as indicated by the red solid arrow in Fig. 1. $\mathbf{J}_S$ increases linearly as a function of $\mathbf{q}$ both in the conventional s-wave [26] and unconventional nodal superconductor [27–29]. However, when the $v_F q$ (where v_F is the Fermi velocity) is comparable to the quasiparticle excitation gap, $\mathbf{J}_S$ reaches a critical current and the superconducting phase becomes unstable [27,28]. In this paper, however, we assume that $\mathbf{J}_S$ is small compared to the critical current; therefore, the supercurrent is proportional to $\mathbf{q}$ (see Supplemental Material [30] for the calculation of J_S as a function of q). Therefore, we utilize $\mathbf{q}$ as a key parameter to describe nonequilibrium states of the superconductor system and plot our main results as a function of $\mathbf{q}$ instead of $\mathbf{J}_S$.

We begin by considering a model lattice Hamiltonian

$$H = H_L + H_R + H_T, \quad (2)$$

where H_L is a doped WSM system and H_R is a metallic s-wave system as depicted in Fig. 1. We assume both of the systems are in superconducting phase and they are weakly coupled by a tunneling Hamiltonian, H_T. We discretize the system in the longitudinal ($\hat{x}$) direction in order to consider a Josephson junction at $x = x_0$ with the tunneling Hamiltonian

$$H_T = \sum_{\mathbf{k},\mathbf{p}} t_{\mathbf{k},\mathbf{p}}[c^\dagger_{\mathbf{k}}(x_0)c_{\mathbf{p}}(x_0) + \mathrm{H.c.}], \quad (3)$$

where $c^\dagger_{\mathbf{k}}$ is the electron creation operator of system H_L, $c_{\mathbf{p}}$ is the annihilation operator of system H_R, $t_{\mathbf{k},\mathbf{p}}$ is a tunneling constant, and $\mathbf{k}$, $\mathbf{p} = (k_y, k_z)$ are momentum of transverse directions. Here, we assume that the tunneling constant is nonzero only at the interface ($x = x_0$).

For the doped WSM system, we choose a model Hamiltonian which breaks time-reversal symmetry but preserves inversion symmetry. Near the Weyl node, we consider a

minimal low-energy two-band model of the WSM [31]

$$H_w = \sum_{\mathbf{k}} \Big[\Big(M - 2 \sum_{\alpha=x,y,z} t_\alpha \cos k_\alpha \Big) \sigma_z + 2\lambda (\sin k_x \sigma_x + \sin k_y \sigma_y) - \mu_L \mathbb{I} \Big], \tag{4}$$

where $\sigma_{x,y,z}$ are the Pauli matrices for spin, $\mathbb{I}$ is the identity matrix, λ is a hopping term in the k_x-k_y plane, and μ_L is the chemical potential in the WSM. In this work, we use a lattice constant of $a = 1$ and set $\hbar = 1$. In Eq. (4), $t_{\alpha=x,y,z}$ is a mass term which determines the position of the Weyl nodes in momentum space. The time-reversal breaking mass term $M = 2t_x + 2t_y + m$ separates Weyl nodes in the system and we set $m = 2t_z \cos Q$ so that two Weyl nodes are located at $\pm\mathbf{Q} = (0,0,\pm Q)$ along the z axis with opposite monopole charge. Assuming FFLO pairing, we consider an attractive Hubbard type interaction. The mean-field approximation for the interaction Hamiltonian is

$$H_{FFLO} = \sum_{\mathbf{k}} [\Delta_{L1} c^\dagger_{\mathbf{k},\uparrow} c^\dagger_{-\mathbf{k}+2\mathbf{Q},\downarrow} + \Delta_{L2} c^\dagger_{\mathbf{k},\uparrow} c^\dagger_{-\mathbf{k}-2\mathbf{Q},\downarrow} + \text{H.c.}], \tag{5}$$

where the first (second) term couples electrons in the FS enclosing the Weyl node located at $k_z = +Q$ $(-Q)$ with a uniform pairing potential Δ_{L1} (Δ_{L2}). To see the finite-size effect of the junction, we discretize the Hamiltonian in the transverse $(\hat{z})$ direction. Therefore, the Hamiltonian of Eqs. (4) and (5) is discretized in the transverse $(\hat{z})$ and longitudinal $(\hat{x})$ directions in real space. As a result, the Bogoliubov–de Gennes (BdG) Hamiltonian is

$$H_L = \sum_{\mathbf{r},k_y} \Phi^\dagger_{r,k_y} \begin{pmatrix} \tilde{H}_w(k_y) & \tilde{H}_{FFLO}(\mathbf{r}) \\ \tilde{H}^\dagger_{FFLO}(\mathbf{r}) & -\tilde{H}^*_w(-k_y) \end{pmatrix} \Phi_{r,k_y} + \sum_{\mathbf{r},\alpha,k_y} \Big[\Phi^\dagger_{r,k_y} \begin{pmatrix} \tilde{H}_{w,\alpha} & 0 \\ 0 & -\tilde{H}^*_{w,\alpha} \end{pmatrix} \Phi_{r+\alpha,k_y} + \text{H.c.} \Big], \tag{6}$$

where $\Phi_{r,k_y} = [c_{\mathbf{r},k_y,\uparrow}, c_{\mathbf{r},k_y,\downarrow}, c^\dagger_{\mathbf{r},-k_y,\uparrow}, c^\dagger_{\mathbf{r},-k_y,\downarrow}]^T$, $\mathbf{r} = (x,z)$, and $\alpha = \delta x, \delta z$. The individual components of the discretized Hamiltonian are

$$\begin{aligned} \tilde{H}_w(k_y) &= [M - 2t_y \cos(k_y a)]\sigma_z + 2\lambda \sin(k_y a)\sigma_y - \mu_L \mathbb{I}, \\ \tilde{H}_{w,\delta x} &= -i\lambda\sigma_x - t_x\sigma_z,\ \tilde{H}_{w,\delta z} = -t_z\sigma_z, \\ \tilde{H}_{FFLO}(\mathbf{r}) &= 2\Delta_L \cos(2Qz) i\sigma_y, \end{aligned} \tag{7}$$

where $\tilde{H}_{w,\delta x}$ and $\tilde{H}_{w,\delta z}$ are the nearest neighbor hopping Hamiltonian in the $\hat{x}$ and $\hat{z}$ directions, respectively, and $\tilde{H}_{FFLO}(\mathbf{r})$ is the superconducting interaction Hamiltonian Fourier transformed to real space. Note that we assume identical pairing potential for each FS, $\Delta_{L1} = \Delta_{L2} = \Delta_L$, but the following arguments are valid regardless of this assumption.

With the Weyl Hamiltonian defined, we consider a normal metal Hamiltonian defined as

$$H_m = \sum_{\mathbf{k}} [-t_m(\cos k_x + \cos k_y + \cos k_z) - \mu_R]\mathbb{I}, \tag{8}$$

where t_m is a hopping term and μ_R is the chemical potential. In our system, the Cooper pairs in the BCS superconductor acquire $\mathbf{q} = q\hat{z}$ through the application of a uniform supercurrent [24,25] in the transverse $(\hat{z})$ direction, as indicated by the red solid arrow in Fig. 1. Then the mean-field approximation to the interaction Hamiltonian is

$$H_{BCS} = \sum_{\mathbf{k}} [\Delta_R c^\dagger_{\mathbf{k}+\mathbf{q}\uparrow} c^\dagger_{-\mathbf{k}+\mathbf{q}\downarrow} + \text{H.c.}], \tag{9}$$

where Δ_R is a uniform BCS pairing potential. The BdG Hamiltonian is constructed for H_R in a similar manner to Eq. (6) and discretized in the transverse $(\hat{z})$ and longitudinal $(\hat{x})$ directions. Consequently,

$$H_R(q) = \sum_{\mathbf{r},k_y} \Phi^\dagger_{r,k_y} \begin{pmatrix} \tilde{H}_m(k_y) & \tilde{H}_{BCS}(\mathbf{r},q) \\ \tilde{H}^\dagger_{BCS}(\mathbf{r},q) & -\tilde{H}^*_m(-k_y) \end{pmatrix} \Phi_{r,k_y} + \sum_{\mathbf{r},\alpha,k_y} \Big[\Phi^\dagger_{r,k_y} \begin{pmatrix} \tilde{H}_{m,\alpha} & 0 \\ 0 & -\tilde{H}^*_{m,\alpha} \end{pmatrix} \Phi_{r+\alpha,k_y} + \text{H.c.} \Big], \tag{10}$$

where the discretized Hamiltonians are

$$\begin{aligned} \tilde{H}_m(k_y) &= (-t_m \cos k_z - \mu_R)\mathbb{I}, \\ \tilde{H}_{m,\delta x} &= -(t_m/2)\mathbb{I},\ \tilde{H}_{m,\delta z} = -(t_m/2)\mathbb{I}, \\ \tilde{H}_{BCS}(\mathbf{r},q) &= \Delta_R e^{i2qz} i\sigma_y. \end{aligned} \tag{11}$$

Here, $\tilde{H}_{m,\delta x}$ and $\tilde{H}_{m,\delta z}$ are the nearest neighbor hopping Hamiltonian and $\tilde{H}_{BCS}(\mathbf{r},q)$ is the interaction Hamiltonian Fourier transformed to real space.

B. Josephson current

Having defined the lattice Hamiltonian for $H_{L/R}$, we may calculate the Josephson current between the doped WSM and s-wave superconductor. Assuming a weak-coupling limit, the tunneling Hamiltonian H_T in Eq. (3) can be treated as a perturbation. From the Ginzburg-Landau theory, we may determine the Josephson current [20]

$$I_J = \text{Im}\Big[t_c \int d\mathbf{r}^2_\parallel \Psi^\dagger_{BCS}(\mathbf{r}_\parallel) \Psi_{FFLO}(\mathbf{r}_\parallel) \Big], \tag{12}$$

where t_c is a coupling constant, and Ψ_{BCS} and Ψ_{FFLO} are order parameters of the s-wave superconductor and doped WSM system, respectively. The integration in Eq. (12) is performed over the interface of the Josephson junction $\mathbf{r}_\parallel = (x_0, y, z)$, whose longitudinal $(\hat{x})$ direction is fixed at the junction position $x = x_0$. Once we put two superconductors together, the order parameters may differ in phase by $\delta\varphi = \varphi_L - \varphi_R$. Taking into account the phase difference, the order parameters in Eq. (12) are rewritten as $\Psi_{FFLO} = \Psi_L(\mathbf{r}_\parallel) e^{i\varphi_L}$ and $\Psi_{BCS} = \Psi_R(\mathbf{r}_\parallel, q) e^{i\varphi_R}$, where Ψ_L and Ψ_R are the order parameters of the doped WSM and s-wave superconductor, respectively. Note that the order parameters Ψ_L and Ψ_R are calculated in *isolated* system as the tunneling Hamiltonian is treated perturbatively. Then, Eq. (12) is rewritten as

$$\begin{aligned} I_J &= \text{Im}\Big[t_c \int d^2\mathbf{r}_\parallel \Psi^\dagger_R(\mathbf{r}_\parallel, q) \Psi_L(\mathbf{r}_\parallel) e^{i\delta\varphi} \Big] \\ &= \text{Im}[I_{J,\max}(q) e^{i\varphi(q)} e^{i\delta\varphi}] \\ &= I_{J,\max}(q) \sin[\varphi(q) + \delta\varphi], \end{aligned} \tag{13}$$

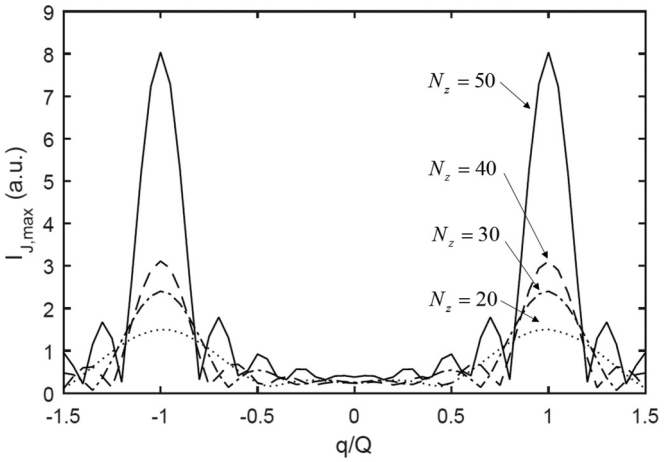

FIG. 2. Plot of Josephson current maximum $I_{J,\max}$ in Eq. (14) as a function of momentum, q, in the BCS superconductor as described by H_R. There are two clear peaks when the q matches with the $\pm Q$ in the doped WSM described by H_L. The parameters $t_m = 1, \mu_R = 0$ are used for H_R and $t_x = 0.5$, $t_y = 0.5$, $t_z = 1.0$, $\lambda = 0.5$, $\mu_L/t = 0.2$, and $Q = 0.1\pi$ are used for H_L. The pairing potentials $\Delta_L/t = \Delta_R/t = 0.2$ are used and the number of points along the longitudinal direction ($\hat{x}$), $N_x = 10$, is fixed for both H_L and H_R. In order to see the finite-size effect of the Josephson junction, we plot $N_z = 20$ to $N_z = 50$.

where $I_{J,\max}$ and $\varphi(q) + \delta\varphi$ are the amplitude and phase of the Josephson current, I_J. We immediately notice that the Josephson current amplitude, $I_{J,\max}$, is a function of momentum q. As is shown in Eq. (7), the interaction Hamiltonian of doped WSM oscillates spatially which manifests as a spatial oscillation in the order parameter Ψ_L. As a result, $I_{J,\max}$ is spatially averaged out and its magnitude vanishes for a sufficiently wide interface ($\gg 1/Q$) at $q = 0$. The situation, however, may be different when a Cooper pair in the s-wave superconductor acquires center-of-mass momentum q by a driven current. The order parameter Ψ_R effectively mimics FFLO states with nonzero momentum q to cancel out the relative spatial variation and, at $q = \pm Q$, $I_{J,\max}$ is restored. To evaluate $I_{J,\max}$, we take a Fourier transform of both order parameters $\Psi_{L/R}$ in the $\hat{y}$ direction

$$I_{J,\max}(q) = \left| t_c \int d^2\mathbf{r}_\parallel \Psi_R^\dagger(\mathbf{r}_\parallel, q)\Psi_L(\mathbf{r}_\parallel) \right| = \left| t_c \int dz \int \frac{dk_y}{2\pi} \Psi_R^\dagger(\mathbf{r}_0, k_y, q)\Psi_L(\mathbf{r}_0, k_y) \right|, \quad (14)$$

where $\mathbf{r}_0 = (x_0, z)$. Then the Hamiltonians in Eqs. (6) and (10) are diagonalized and the order parameters $\Psi_L(\mathbf{r}, k) = \langle c_{\uparrow,\mathbf{r},k} c_{\downarrow,\mathbf{r},-k} \rangle_L$ and $\Psi_R(\mathbf{r}, k, q) = \langle c_{\uparrow,\mathbf{r},k} c_{\downarrow,\mathbf{r},-k} \rangle_R$ are evaluated (see the Appendix). In Fig. 2, we plot $I_{J,\max}$ calculated from Eq. (14). We see a clear peak in $I_{J,\max}$ at $q = \pm Q$ where the momentum q in the BCS superconductor cancels the momentum Q carried by FFLO states in the WSM. The oscillations in $I_{J,\max}$ are due to the finite size of the lattice having an insufficient sampling of k space. The width of the peak is decreased as we increase the resolution of the momentum space by increasing the system size. The peak is ideally a delta function at $q = \pm Q$ if the junction size is large enough to satisfy $\Delta k = 2\pi/L_z \ll Q$. In the presence of weak disorder, the peak may be shifted as disorder renormalizes the mass term of the WSM Hamiltonian [32], but persists as the FFLO states discussed here are robust to impurity scattering [10]. Therefore, the Josephson current amplitude at nonzero transverse ($\hat{z}$) current ($q \neq 0$) may serve as a signature of FFLO states for inversion-symmetric doped WSMs.

III. PROBING NODAL SUPERCONDUCTIVITY

While intranode superconducting states are identified by quantum transport signatures in the Josephson junction, applying the same method may not confirm internode superconducting states as nodal BCS states do not carry finite momentum and the current response simply returns to conventional Josephson junction results. Instead, we exploit nodal structures of inversion-symmetric doped WSMs [10,16,17,33] and propose a separate quantum transport method to identify nodal BCS superconductivity using a four-terminal measurement.

A. Nodal BCS states in doped WSMs

As the only prerequisite for nodal superconductivity in doped WSMs is the presence of inversion symmetry [17], the internode pairing results in nodal superconductivity even in the presence of a uniform BCS pairing potential. Each nodal point carries topologically nontrivial *vorticity* inherited from the monopole charge of the corresponding FS in the normal phase [17]. Therefore, each nodal point exhibits similar physics with that of the WSM such as Fermi arcs [13,16,17]. In addition, the nodal BCS superconductivity facilitates a zero energy flat band dispersion at its surface that is protected by mirror symmetry [10,16,17]. The flat band zero energy can be experimentally confirmed by zero bias conductance peak at the surface [16] and may serve as evidence of nodal superconductivity. However, seeking the zero bias peak may be a difficult task due to the gapless bulk conducting channels [34]. Instead, we propose to utilize an induced topological phase transition by application of current through the superconducting system. Here, we show that the nodal points, initially assumed to be well separated in equilibrium, are shifted in momentum space by a uniform supercurrent. Then nodal pair annihilation may occur and the subsequent phase transition depletes available bulk states within the superconducting gap. As a result, the phase transition is captured by a distinct dip in the density of states (DOS or dI/dV) and an observation of the dip in nonequilibrium may serve as a signature of nodal BCS superconductivity in doped WSMs.

B. Nodal pair annihilation and energy spectrum

To examine the induced topological transition, we assume a four-terminal device setup outlined in Fig. 3(a). The red solid arrow in Fig. 3(a) represents a uniform supercurrent driven by an external current source, which induces a net momentum shift of Cooper pairs by a momentum q in the transverse ($\hat{z}$) direction. In the following argument, we show that the momentum q shifts nodal points in momentum space to induce a topological phase transition. To observe the corresponding topological phase transition, we utilize the DOS by measuring

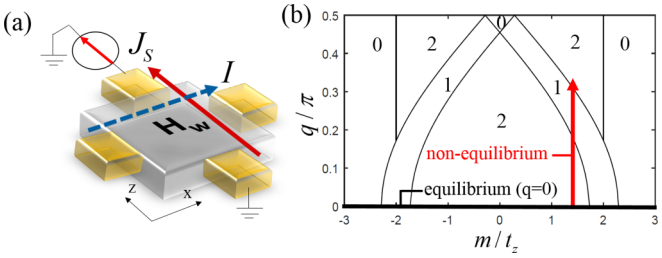

FIG. 3. (a) A schematic of the system. Uniform supercurrent J_S is driven to the Weyl superconductor system H_w. Differential conductance is read from a current measured in perpendicular direction (I). (b) Phase diagram of the number of nodal point pairs from Hamiltonian Eq. (15) at $k_x = k_y = 0$. A DOS is obtained in the particular direction indicated by the red vertical arrow and plotted in Fig. 4. For the WSM Hamiltonian, the same parameters used in Fig. 2 are adopted. The range of q presented here is $0 \leqslant q \leqslant \pi/2$ due to the fact that a relevant range of total Cooper pair momentum is $|2q| \leqslant \pi$.

a differential conductance in the longitudinal ($\hat{x}$) direction shown as a blue dashed arrow in Fig. 3(a). For inversion-symmetric doped WSMs, we use the lattice WSM Hamiltonian $H_w = \sum_{\mathbf{k}} \tilde{H}_w(\mathbf{k})$ in Eq. (4) with shifted center-of-mass frame by q to account for uniform supercurrent. Assuming uniform BCS pairing, the BdG Hamiltonian is

$$H_{\mathrm{BdG}} = \sum_{\mathbf{k},q} \Phi^{\dagger}_{\mathbf{k},q} \begin{pmatrix} \tilde{H}_w(\mathbf{k}+q) & \tilde{H}_{BCS} \\ \tilde{H}^{\dagger}_{BCS} & -\tilde{H}^{*}_{w}(-\mathbf{k}+q) \end{pmatrix} \Phi_{\mathbf{k},q}, \tag{15}$$

where $\Phi_{\mathbf{k},q} = [c_{\mathbf{k}+q,\uparrow}, c_{\mathbf{k}+q,\downarrow}, c^{\dagger}_{-\mathbf{k}+q,\uparrow}, c^{\dagger}_{-\mathbf{k}+q,\downarrow}]$. In this shifted center-of-mass frame, the mean-field interaction Hamiltonian is defined as $\tilde{H}_{BCS} = \Delta_0 i\sigma_y$, where Δ_0 is a uniform pairing potential. The position of the nodal points in Eq. (15) is determined by considering the quasiparticle spectrum along the k_z axis. For illustrative purposes, we analyze the Hamiltonian in Eq. (4) along the k_z direction, which is $\tilde{H}_w(k_z) = [m - 2t_z \cos(k_z)]\sigma_z - \mu\mathbb{I}$, by setting $k_x = k_y = 0$. Then, Eq. (15) may be rewritten in a block diagonal form as $\begin{pmatrix} \tilde{H}_{\uparrow\downarrow} & 0 \\ 0 & \tilde{H}_{\downarrow\uparrow} \end{pmatrix}$, whose bases in each block are $[c_{\mathbf{k}+q,\uparrow}, c^{\dagger}_{-\mathbf{k}+q,\downarrow}]$ and $[c_{\mathbf{k}+q,\downarrow}, c^{\dagger}_{-\mathbf{k}+q,\uparrow}]$, respectively. The quasiparticle spectrum along the k_z axis is

$$\begin{aligned} E^{\pm}_{\uparrow\downarrow}(k_z,q) &= (m - 2t_z \cos k_z \cos q) \\ &\quad \pm \sqrt{\Delta_0^2 + (\mu - 2t_z \sin k_z \sin q)^2}, \\ E^{\pm}_{\downarrow\uparrow}(k_z,q) &= (2t_z \cos k_z \cos q - m) \\ &\quad \pm \sqrt{\Delta_0^2 + (\mu + 2t_z \sin k_z \sin q)^2}. \end{aligned} \tag{16}$$

In Eq. (16), the nodal points are found at the crossings of the quasiparticle spectra. To see the nodal point dependency on q, we further simplify Eq. (16) by assuming $\mu = 0$ and setting the mass term to be $m = 2t_z \cos Q$ to place Weyl nodes at $k_z = \pm Q$. We then expand the quasiparticle spectrum around $\pm Q$. Specifically, we set $k_z = \pm Q + \delta k_z$ where $\delta k_z \ll Q$ is an infinitesimal deviation from a location of the Weyl node in normal phase. Assuming a small q ($q \ll Q$) we obtain

$$\begin{aligned} E_{+}(\delta k_z, q) &\simeq \left[t'_z \delta k_z \pm \sqrt{\Delta_0^2 + t'^2_z q^2}\right]\sigma_z, \\ E_{-}(\delta k_z, q) &\simeq \left[-t'_z \delta k_z \pm \sqrt{\Delta_0^2 + t'^2_z q^2}\right]\sigma_z, \end{aligned} \tag{17}$$

where $E_{\pm}$ is the quasiparticle spectrum in the vicinity of $k_z = \pm Q$. In Eq. (17), we set $t'_z = 2t_z \sin Q$ and σ_z is the Pauli matrix in pseudospin space whose components consist of linear combinations of the eigenfunctions in Eq. (16). Equation (17) shows that each FS has two nodal points at $\delta k_z = \pm\sqrt{(\Delta_0/t'_z)^2 + q^2}$ and the nodal points are shifted as a function of q toward $k_z = 0$ and π. Due to the particle-hole symmetry, we know that a nodal point pair exists at $(k_z, E) = (k_0, E_0)$ and $(-k_0, -E_0)$, and the pair consists of opposite vorticity by inversion symmetry of the WSM. Therefore, by manipulating q, the nodal pair with opposite vorticity may be shifted to be annihilated at $k_z = 0$ or $\pm\pi$ and the total number of nodal point pairs given by the band topology at equilibrium can be tuned. In Fig. (3 b), the phase diagram of the system that contains a different number of nodal point pairs is shown as a function of the mass term m and momentum q, which determines the position of nodal points in equilibrium and nonequilibrium, respectively. The wave vector q is controlled by applied current and m is determined by the magnetic order of material or magnetized impurities. When $q = 0$, the system contains two nodal point pairs for $|m| \leqslant 2t_z - \sqrt{\Delta_0^2+\mu^2}$. If the normal phase of the WSM has Weyl node separation smaller than $2Q \leqslant \sqrt{\Delta_0^2+\mu^2}$ in momentum space, a pair of nodal points is annihilated as one turns on the superconductivity and, as a result, only one nodal point pair remains in the system. When $|m| \geqslant 2t_z + \sqrt{\Delta_0^2+\mu^2}$, the system is fully gapped and no nodal point pairs exist. Departing from equilibrium, nodal points are shifted and annihilated by increasing q, for example, as shown in the red vertical arrow in Fig. 3(b). Although this phase transition may not be observed if the nodal point separation is larger than the maximum accessible range of the supercurrent, we believe that proposed experimental setup is applicable as the position of the Weyl node may be adjusted, for example in multilayer structure [35,36], by tuning the concentration of magnetic impurities or the thickness of each layer. Note that we only consider a phase diagram when $(k_x, k_y) = (0,0)$. The same arguments are also valid for other high-symmetry points in the Brillouin zone such as $(k_x, k_y) = (\pm\pi, \pm\pi)$ which simply replaces the mass term $m \to m + 4t_x$ for $(\pm\pi, 0)$, $m + 4t_y$ for $(0, \pm\pi)$, and $m + 4t_x + 4t_y$ for $(\pm\pi, \pm\pi)$. Nonetheless, the resulting physics is identical.

C. Signatures of the phase transition

When the phase transition occurs under nonequilibrium conditions, the annihilated nodal pairs no longer provide available states within the superconducting gap. As a result, the induced topological transition is observed in the DOS (or dI/dV). To examine this, we compute DOS(E,q) as a function of energy and momentum q using the system Green's function [37]. Note that the system boundary in the y direction is open in real space so that we may observe finite-size effects and the surface states contribution. To examine the induced topological phase transition and the corresponding DOS, we sweep q at an arbitrary cut of the phase diagram at $m/t_z =$

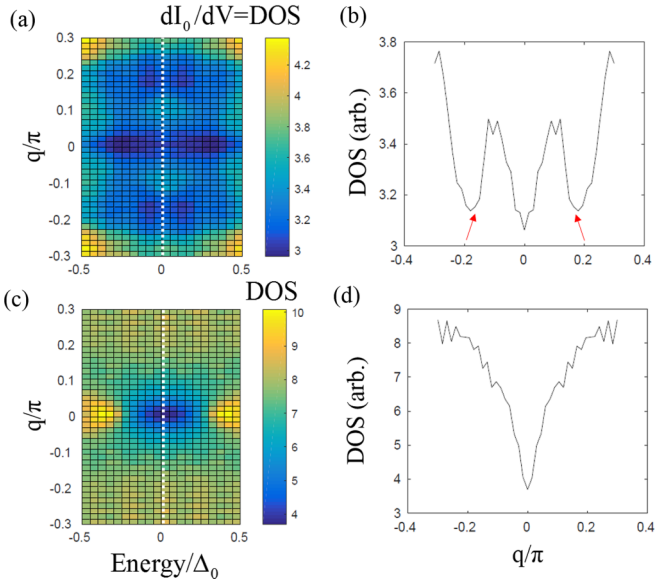

FIG. 4. A DOS plot along the vertical red arrow in Fig. 3(b). (a) DOS is plotted as a function of q within a superconducting gap. Pairing potential is set to be $\Delta_0/t_z = 0.2$ with (a) $N_y = 50$ and (c) $N_y = 5$. A chemical potential is $\mu/t_z = 0.2$. (b) DOS plot at $E = 0$ as a function of q for $N_y = 50$ [white dotted line in (a)]. (d) DOS plot at $E = 0$ as a function of q for $N_y = 5$ [white dotted line in (c)].

$2\cos(Q = 0.2\pi) \simeq 1.6$. As the red arrow in Fig. 3(b) shows, the phase transition occurs around $q/\pi \simeq 0.1$. Figure 4(a) shows the corresponding DOS where we set the thickness to $N_y = 50$ to avoid finite-size effects. Along the horizontal axis at $q = 0$ in Fig. 4(a), equilibrium DOS increases quadratically in energy ($\propto E^2$) within the superconducting gap due to the presence of bulk nodal points, whereas surface states result in nonzero DOS near $E = 0$. When the system is not in equilibrium ($q \neq 0$), the eigenstates initially separated by a superconducting gap are shifted by q and added to the available low-energy states [28]. As a result, DOS increases as a function of q. However, there are distinct drops in magnitude of DOS at certain q as is seen by following vertical axis in Fig. 4(a). With this particular choice of mass (m) in the phase diagram, a pair of nodal points with opposite vorticity moves toward $k_z = 0$ and is annihilated at $q/\pi \simeq 0.1$. Further increase in q from this point gaps out the spectrum at $k_z = 0$ and a topological phase transition occurs leaving only one pair of nodal point pairs in the system. Thus, the available states within the superconducting gap are decreased and the consequent change in nodal structure manifests itself as a dip in the DOS. The dip is clearly observed in the zero-energy cut indicated with red arrows in Fig. 4(b). Therefore, the distinct dip of the DOS in nonequilibrium is a signature of the quantum critical point which can only occur due to the topological phase transition of the nodal superconductor. Note that above arguments are valid for a system where the bulk nodal points are well defined so that their annihilation can be clearly identified. If the bulk nodal points are gapped out by the finite-size effect, the signature may not be obvious in the DOS. Figure 4(c) shows a DOS for a thickness of $N_y = 5$ where the bulk states are gapped out by the finite-size effect. The DOS within the finite-size induced gap is suppressed but finite due to an infinitesimal broadening we introduced in the Green's function calculation [37] and surface states with hybridization gap $E/\Delta \simeq 0.5$. Consequently, in Fig. 4(d), we observe a monotonic increase of DOS as a function of q and no clear signature of nodal point annihilation is observed.

IV. SUMMARY AND CONCLUSION

In summary, we study two complementary quantum transport methods to probe FFLO and nodal BCS states in the superconducting phase of the inversion-symmetric doped WSM. To identify FFLO states, we consider a Josephson junction consisting of a doped WSM and conventional s-wave superconductor. When the junction is in the weak-coupling limit, the Josephson current is calculated from the order parameters in the lattice Hamiltonian using Ginzburg-Landau theory. The order parameter of the doped WSM oscillates spatially due to the finite momentum, Q, carried by FFLO states that results in a vanishing Josephson current. By driving a uniform current in a conventional s-wave superconductor, the order parameter of the s-wave superconductor effectively mimics FFLO states carrying a net momentum q. When the modulated order parameter effectively cancels Q at $q = \pm Q$, a finite Josephson current is restored. Therefore, the peak in Josephson current in nonequilibrium serves as a direct signature of the presence of FFLO states in doped WSMs.

Additionally, we show that protected nodal points in equilibrium may be shifted by using four-contact quantum transport geometry on doped WSMs. The system may undergo an induced topological transition by annihilating the nodal point pairs, which is signalled by an abrupt changes in the DOS (or differential conductance). Using a lattice model and Green's function, we observe a distinct dip in DOS as one across a boundary of the phase diagram where a nodal point pair annihilation occurs. Thus, the induced topological phase transition and corresponding signatures in the DOS at nonequilibrium may serve as an indication of the nodal superconductivity in doped WSMs.

ACKNOWLEDGMENTS

M.J.P. and M.J.G. acknowledge financial support from the National Science Foundation (NSF) under Grant No. CAREER EECS-1351871. M.J.P. and Y.K. acknowledge useful discussions with Timothy Philip and Yuxuan Wang. M.J.P. acknowledges fruitful discussions with David ChangMo Yang and Gil Young Cho.

APPENDIX: ORDER PARAMETER CALCULATION

In this Appendix, we summarize the method utilized to obtain the order parameter in Eq. (14) from the BdG Hamiltonian. The Hamiltonians in Eq. (6) and (10) are discretized in the $r = (x,z)$ direction with a momentum k in the $\hat{y}$ direction. Then the Hamiltonian can be diagonalized from the following Bogoliubov transform [24]:

$$\begin{pmatrix} c_{r,k,\sigma} \\ c^{\dagger}_{r,-k,\bar{\sigma}} \end{pmatrix} = \sum_n \begin{pmatrix} u_{n,r,k} & -v^{*}_{n,r,k} \\ v_{n,r,k} & u^{*}_{n,r,k} \end{pmatrix} \begin{pmatrix} \gamma_{\alpha,n,r,k} \\ \gamma^{\dagger}_{\beta,n,r,k} \end{pmatrix} = \sum_n R_{n,k,z} \begin{pmatrix} \gamma_{\alpha,n,k,z} \\ \gamma^{\dagger}_{\beta,n,k,z} \end{pmatrix}, \quad \text{(A1)}$$

where $\sigma = \uparrow, \downarrow$ is the spin index and $\bar{\sigma}$ stands for an opposite spin with σ and a quasiparticle operator index $(\alpha,\beta) = (1,2)$ for $\sigma = \uparrow$ and $(3,4)$ for $\sigma = \downarrow$ for each eigenstate index n. Here, we define a basis rotation matrix $R_{n,r,k}$ which diagonalizes the Hamiltonian

$$H(r,k)R_{n,r,k} = R_{n,r,k}\begin{pmatrix} E_{n,r,k} & 0 \\ 0 & -E_{n,r,k} \end{pmatrix}. \quad \text{(A2)}$$

Therefore, we obtain the rotation matrix $R_{n,k,z}$ and corresponding eigenvalue $E_{n,r,k}$ by diagonalizing the Hamiltonian in Eqs. (6) and (10). Then, an order parameter with uniform s-wave pairing potential is defined as

$$\Psi(r,k) = \langle c_{r,k,\uparrow} c_{r,-k,\downarrow} \rangle. \quad \text{(A3)}$$

The quasiparticle operator γ satisfies the commutation relation $\gamma^{\dagger}_{\alpha,n}\gamma_{\alpha',m} + \gamma_{\alpha',m}\gamma^{\dagger}_{\alpha,n} = \delta_{n,m}\delta_{\alpha,\alpha'}$ and $\gamma_{\alpha,n}\gamma_{\alpha',m} + \gamma_{\alpha',m}\gamma_{\alpha,n} = 0$ for $\alpha,\alpha' = 1,2,3,4$. Then we can plug Eq. (A1) into Eq. (A3) and obtain

$$\langle c_{r,k,\sigma} c_{r,-k,\bar{\sigma}} \rangle = \sum_n u_n v^*_n \langle 1 - \gamma^{\dagger}_{\alpha,n}\gamma_{\alpha,n} - \gamma^{\dagger}_{\beta,n}\gamma_{\beta,n} \rangle, \quad \text{(A4)}$$

where we used the commutation relation of γ and we have suppressed the r,k, $\uparrow\downarrow$ index on the right-hand side of Eq. (A4) for brevity. For finite temperature, $\langle \gamma^{\dagger}_{\alpha,n}\gamma_{\beta,m} \rangle = \delta_{n,m}\delta_{\alpha,\beta} f(E_n)$ and $\langle \gamma_{\alpha,n}\gamma_{\beta,m} \rangle = 0$, where $f(E)$ is the Fermi-Dirac distribution. Therefore, we obtain the s-wave pairing order parameter in Eq. (A3),

$$\begin{aligned} \Psi(r,k) &= \langle c_{r,k,\uparrow} c_{r,-k,\downarrow} \rangle \\ &= \sum_n u_{n,r,k} v^*_{n,r,k} [1 - 2f(E_{n,r,k})] \\ &= \sum_n u_{n,r,k} v^*_{n,r,k} \tanh \frac{E_{n,r,k}}{2k_B T}, \end{aligned} \quad \text{(A5)}$$

and the resultant mean-field pairing Hamiltonian is then

$$H_{\text{int}} = \sum_{r,k} \Delta(r,k) c^{\dagger}_{r,k,\uparrow} c^{\dagger}_{r,-k,\downarrow} + \text{H.c.}, \quad \text{(A6)}$$

where $\Delta(r,k) = g\Psi(r,k)$ and $g > 0$ is an attractive interaction strength for the order parameter definition of Eq. (A3).

[1] S. Murakami, New J. Phys. **9**, 356 (2007).
[2] X. Wan, A. M. Turner, A. Vishwanath, and S. Y. Savrasov, Phys. Rev. B **83**, 205101 (2011).
[3] C.-K. Chiu and A. P. Schnyder, Phys. Rev. B **90**, 205136 (2014).
[4] Z. Fang, N. Nagaosa, K. S. Takahashi, A. Asamitsu, R. Mathieu, T. Ogasawara, H. Yamada, M. Kawasaki, Y. Tokura, and K. Terakura, Science **302**, 92 (2003).
[5] H. Nielsen and M. Ninomiya, Nucl. Phys. B **185**, 20 (1981).
[6] H. Nielsen and M. Ninomiya, Nucl. Phys. B **193**, 173 (1981).
[7] R. Okugawa and S. Murakami, Phys. Rev. B **89**, 235315 (2014).
[8] S.-Y. Xu, I. Belopolski, N. Alidoust, M. Neupane, G. Bian, C. Zhang, R. Sankar, G. Chang, Z. Yuan, C.-C. Lee *et al.*, Science **349**, 613 (2015).
[9] P. Hosur and X. Qi, C. R. Phys. **14**, 857 (2013).
[10] G. Y. Cho, J. H. Bardarson, Y.-M. Lu, and J. E. Moore, Phys. Rev. B **86**, 214514 (2012).
[11] H. Wei, S.-P. Chao, and V. Aji, Phys. Rev. B **89**, 014506 (2014).
[12] G. Bednik, A. A. Zyuzin, and A. A. Burkov, Phys. Rev. B **92**, 035153 (2015).
[13] T. Zhou, Y. Gao, and Z. D. Wang, Phys. Rev. B **93**, 094517 (2016).
[14] P. Hosur, X. Dai, Z. Fang, and X.-L. Qi, Phys. Rev. B **90**, 045130 (2014).
[15] T. Meng and L. Balents, Phys. Rev. B **86**, 054504 (2012).
[16] B. Lu, K. Yada, M. Sato, and Y. Tanaka, Phys. Rev. Lett. **114**, 096804 (2015).
[17] Y. Li and F. D. M. Haldane, arXiv:1510.01730.
[18] P. Fulde and R. A. Ferrell, Phys. Rev. **135**, A550 (1964).
[19] A. I. Larkin and Yu. N. Ovchinnikov, Zh. Eksp. Teor. Fiz. **47**, 1136 (1964) [Sov. Phys. JETP **20**, 762 (1965)].
[20] K. Yang and D. F. Agterberg, Phys. Rev. Lett. **84**, 4970 (2000).
[21] P. E. C. Ashby and J. P. Carbotte, Phys. Rev. B **87**, 245131 (2013).
[22] A. Maldonado, I. Guillamón, H. Suderow, and S. Vieira, Rev. Sci. Instrum. **82**, 073710 (2011).
[23] A. Maldonado, S. Vieira, and H. Suderow, Phys. Rev. B **88**, 064518 (2013).
[24] P. D. Gennes, *Superconductivity of Metals and Alloys* (W. A. Benjamin, New York, 1966).
[25] M. Tinkham, *Introduction to Superconductivity* (McGraw-Hill Inc., New York, 1996).
[26] J. Bardeen, Rev. Mod. Phys. **34**, 667 (1962).
[27] D. Zhang, C. S. Ting, and C.-R. Hu, Phys. Rev. B **70**, 172508 (2004).
[28] I. Khavkine, H.-Y. Kee, and K. Maki, Phys. Rev. B **70**, 184521 (2004).
[29] H.-Y. Kee, Y. B. Kim, and K. Maki, Phys. Rev. B **70**, 052505 (2004).
[30] See Supplemental Material at http://link.aps.org/supplemental/10.1103/PhysRevB.93.214511 for the calculation of J_S as a function of q.
[31] K.-Y. Yang, Y.-M. Lu, and Y. Ran, Phys. Rev. B **84**, 075129 (2011).
[32] H. Shapourian and T. L. Hughes, Phys. Rev. B **93**, 075108 (2016).
[33] G. B. Halász and L. Balents, Phys. Rev. B **85**, 035103 (2012).
[34] A. Chen and M. Franz, Phys. Rev. B **93**, 201105 (2016).
[35] A. A. Zyuzin, S. Wu, and A. A. Burkov, Phys. Rev. B **85**, 165110 (2012).
[36] A. A. Burkov and L. Balents, Phys. Rev. Lett. **107**, 127205 (2011).
[37] S. Datta, *Quantum Transport: Atom to Transistor* (Cambridge University Press, New York, 2005).